



Intramolecular π -stacked Perylene-Diimide Acceptors for Non-fullerene Organic Solar Cells

Journal:	<i>Journal of Materials Chemistry A</i>
Manuscript ID	TA-COM-01-2019-000343.R1
Article Type:	Communication
Date Submitted by the Author:	05-Mar-2019
Complete List of Authors:	Zhang, Jianquan; The Hong Kong University of Science and Technology, Chemistry Bai, Fujin; The Hong Kong University of Science and Technology, Department of Chemistry Li, Yunke; The Hong Kong University of Science and Technology, Department of Chemistry Hu, Huawei; North Carolina State University, Physics; North Carolina State University, Physics Liu, Bin; The Hong Kong University of Science and Technology, Department of Chemistry Zou, Xinhui; The Hong Kong University of Science and Technology, Department of Chemistry Yu, Han; The Hong Kong University of Science and Technology, Chemistry Huang, Jiachen; Hong Kong University of Science and Technology Pan, Ding; Department of Physics, the Hong Kong University of Science and Technology, Clear Water Bay, Hong Kong, China; Department of Chemistry, the Hong Kong University of Science and Technology, Clear Water Bay, Hong Kong, China; HKUST Fok Ying Tung Research Institute, Guangzhou, China Ade, Harald; North Carolina State University, Department of Physics Yan, He; The Hong Kong University of Science and Technology, Department of Chemistry

Intramolecular π -stacked Perylene-Diimide Acceptors for Non-fullerene Organic Solar Cells

Jianquan Zhang,^{†,§} Fujin Bai,[§] Yunke Li,[§] Huawei Hu,[#] Bin Liu,[‡] Xinhui Zou,[§] Han Yu,[§] Jiachen Huang,[§] Ding Pan,[‡] Harald Ade,^{#,*} He Yan^{†,§*}

[†] Hong Kong University of Science and Technology-Shenzhen Research Institute, No. 9 Yuexing 1st RD, Hi-tech Park, Nanshan, Shenzhen 518057, P. R. China

[§] Department of Chemistry and Hong Kong Branch of Chinese National Engineering Research Center for Tissue Restoration & Reconstruction, Hong Kong University of Science and Technology (HKUST), Clear Water Bay, Kowloon, Hong Kong, China

[‡] Department of Physics and Department of Chemistry, Hong Kong University of Science and Technology (HKUST), Clear Water Bay, Kowloon, Hong Kong, China

[#] Department of Physics and Organic and Carbon Electronics Laboratory, North Carolina State University, Raleigh, NC 27695, USA

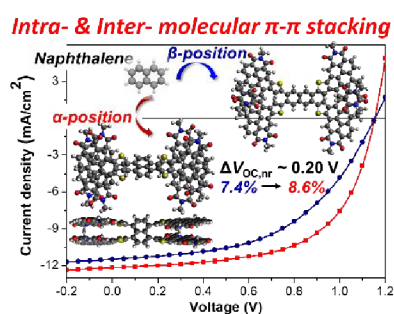
Corresponding Author

* Email: hyan@ust.hk (He Yan); harald_ade@ncsu.edu (Harald Ade)

Abstract

Proper molecular packing is the key to improve the performances of non-fullerene organic solar cells (OSCs) based on perylene diimides (PDI). Herein, we implement a novel concept of introducing intramolecular π - π stacking for the design of PDI-based acceptors. We synthesized and systematically studied two isomeric PDI-tetramers with different functionalization positions (α - and β -positions) of naphthalene, and thus different extent of intramolecular packing. Interestingly, both PDI molecules exhibit two π - π stacking peaks with intramolecular and intermolecular stacking distances of 3.7-3.8 Å and 4.6-4.7 Å, respectively. Most importantly, the α -positioned PDI show stronger intramolecular π -stacked features as evidenced by UV-Vis and photoluminescence, and morphological measurements. Consequently, the α -positioned PDI achieved a higher device efficiency of 8.6% with an open-circuit voltage of 1.15 V and a reasonably high fill factor of 60%. Our work highlights the importance of intramolecular π - π stacking in the design of novel PDI-based SMAs.

TOC graph



Two isomeric perylene diimide acceptors with both intra- and intermolecular π - π stacking are developed for non-fullerene organic solar cells.

Introduction

Great progress has been made in the field of organic solar cells (OSCs) in recent years, which can be mainly attributed to the development of non-fullerene acceptors and matching donor polymers.¹⁻⁶ Tremendous research efforts have been dedicated to the molecular design of small molecular acceptors (SMAs) due to their low-cost synthesis, readily tunable absorption and energy levels, as well as morphological compatibility with different types of donor materials.⁷⁻¹³ Perylene diimides (PDI) are one of the promising electron-withdrawing building blocks to construct high-performance SMAs, owing to their easy accessibility, high electron affinity and mobility and intense absorption in the visible region.¹⁴⁻¹⁷

One of the design rationales for PDI-based SMAs is to introduce three-dimensional geometries with a sterically congested aromatic core flanking three or more PDI wings resembling a “propeller”.¹⁸⁻²³ The highly twisted molecular geometry breaks the planarity of PDI molecules, which greatly alleviates the excessive intermolecular aggregation of PDIs that form micron-sized phase segregation when blended with donor polymers.²⁴ Although improved bulk heterojunction (BHJ) morphology with small domain sizes can be obtained via this strategy, the electron mobilities of these highly twisted PDI molecules as well as the fill factors (FF) of the devices inevitably decrease.^{7,20} This is because the crowded aromatic cores separate the flanking PDI units far away from each other, which hinders not only intermolecular but also intramolecular electronic interactions that are equally important for efficient electron transport processes.^{25,26} An intuitive thought is how the concept of intramolecular π -stacked PDI molecules can be applied to the field of OSCs, as it would provide an extra pathway for electron transport and positive effects on the optical and morphological properties of PDI-based devices. Previously, enforcing intramolecular π -stacks by rational design of the core structure of PDI molecules has been shown to dramatically affect the electronic and vibrational coupling between the adjacent PDI subunits.²⁷ The “folding” geometries of PDIs exhibit unique optical and electronic properties that provide in-depth insight into self-assembly behavior, charge and energy transfer processes of chromophores.²⁸⁻³⁴ Nonetheless, these intramolecular π -stacked PDI molecules were primarily designed for the

purpose of fundamental studies instead of OSC operation, and therefore, to the best of our knowledge, few efficient OSC devices were reported based on this type of acceptors. This encourages us to explore novel core structures for constructing intramolecular π -stacked PDI molecules to reveal the structure-property-performance relationship, which is of great interest and importance to the OSC field.

Herein, we report the synthesis, characterizations and device performances of two isomeric PDI-based SMAs based on the novel tetrathienynaphthalene (TTN) cores and show how the extent of intramolecular π -stacking affect the photovoltaic performances of PDI-based SMAs. The two PDI molecules are different in the functionalization positions of the naphthalene ring, i.e., α - and β -positions (**Figure 1a**). Most importantly, morphological studies show that both molecules exhibit two distinct π - π stacking modes, which are assigned to intra- and intermolecular stacking. Theoretical calculations reveal that the α -isomer (a-FTTN-PDI4) features a “double-decker” geometry containing two pairs of intramolecular π -stacked PDI units, while the PDI units of the β -isomer (b-FTTN-PDI4) show a lower extent of overlapping. The different intramolecular π -stacking of these two PDI molecules was evidenced by UV-Vis and time-resolved photoluminescence spectra. In addition, better molecular packing (larger coherence length) is observed for a-FTTN-PDI4, which lead to higher electron mobility and domain purity in the blend film. Consequently, the devices based on a-FTTN-PDI4 showed the highest power conversion efficiency of 8.6% with a high open-circuit voltage of 1.15 V, which outperformed that of b-FTTN-PDI4 (7.4%). As far as we know, this work is the first report on efficient devices based on intramolecular π -stacked PDIs and highlights the significance of simultaneously enhancing intra- and intermolecular packing for improving the device performances of PDI-based SMAs.

Results and Discussion

The details of the synthesis of the two SMAs were summarized in the **Supporting Information**. All compounds were identified by NMR, mass spectra and elementary analysis. Their thermal stability was evaluated by using thermogravimetric analysis (TGA), as shown in **Figure S1** in the Supporting Information. The decomposition temperatures at 5% weight loss are higher than 350 °C for both SMAs, indicative of their good thermal stability for photovoltaic applications. In

addition, no obvious crystallization or melting peaks can be observed for both PDI molecules in the differential scanning calorimetry (DSC, **Figure S2**) measurements, suggesting their mostly amorphous nature.

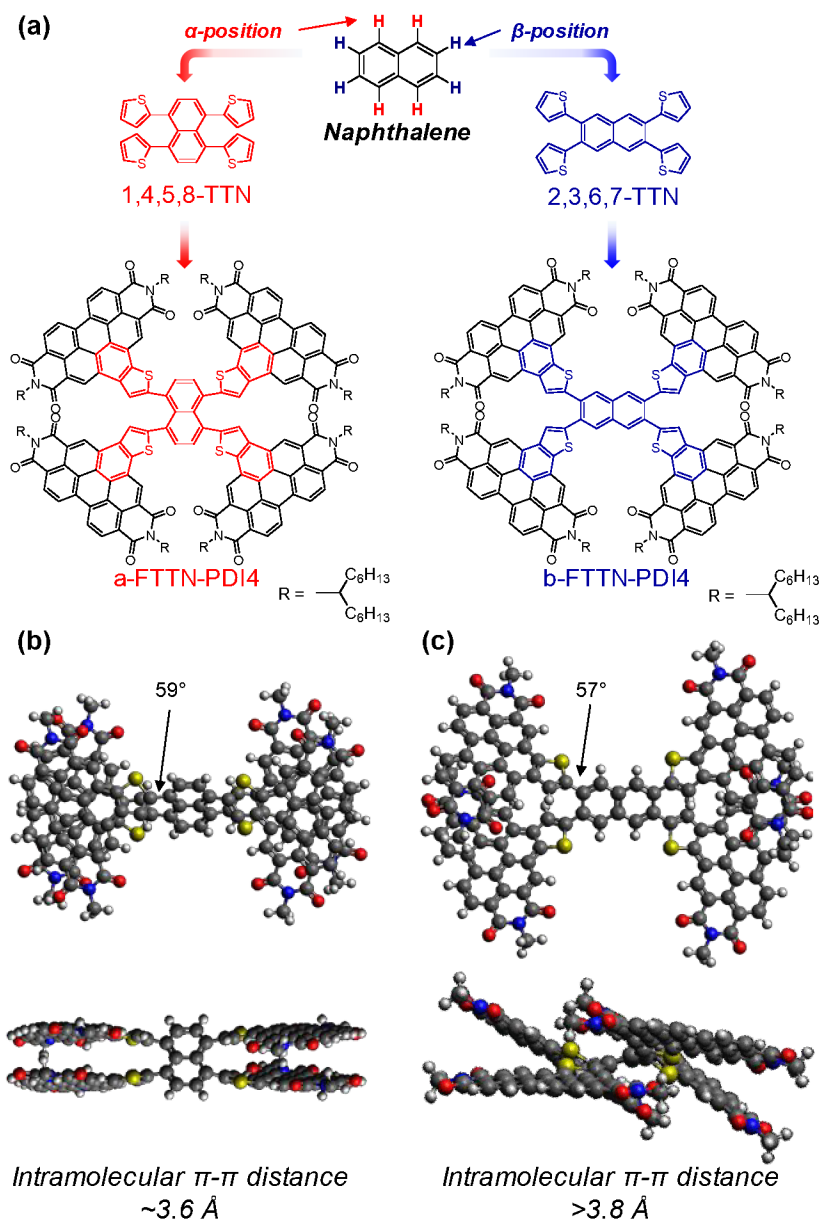


Figure 1. (a) Chemical structures of naphthalene, (α - and β -positions are marked by red and blue, respectively), 1,4,5,8-tetrathienylnaphthalene (a-TTN) and 2,3,6,7-tetrathienylnaphthalene (b-

TTN) and the PDI-based derivatives: a-FTTN-PDI4 and b-FTTN-PDI4. Optimized molecular geometries of (b) a-FTTN-PDI4 and (c) b-FTTN-PDI4.

To gain insight into the differences in their molecular geometries, theoretical calculations were performed with the alkyl chains replaced by methyl groups for simplification. The detailed calculation method and the Cartesian coordinates of two SMAs were demonstrated in the supporting information. As shown in **Figure 1b**, the α -positions on the same side of the naphthalene ring are parallel and close to each other, which would create large steric hindrance between the adjacent PDI units attached to these positions.³⁵ Therefore, the adjacent PDI units of a-FTTN-PDI4 are forced to adopt a “face-to-face” conformation with an interchromophore distance of ~ 3.6 Å. Notably, we tried different initial conformation of a-FTTN-PDI4, and all the optimized geometries consistently exhibited similar intramolecular π -stacked conformations (**Figure S3**). In contrast to a-FTTN-PDI4, the larger distance between the β -positions compared with the α -positions of the naphthalene ring posed less steric hindrance between the adjacent PDI units, which may allow conformational changes to other low-energy conformations rather than the co-facially stacked one (**Figure 1c**). As a result, the optimal geometry of b-FTTN-PDI4 exhibits a less extent of intramolecular π -stacking with partial overlap of the adjacent PDI units resembling a “head-to-tail” arrangement, and a larger interchromophore distance of >3.8 Å.

To verify the existence of intramolecular π -stacking, UV-Vis measurements of the PDI molecules were performed, as they are known to be sensitive to the interchromophore distance and orientation.^{14, 27} To obtain deeper insight into the intramolecular interactions of these two SMAs, the referencing molecule, thiophene-fused PDI named PDIT (**Figure 2a**), was also synthesized and involved in the comparisons. The absorption spectra of PDIT, a-FTTN-PDI4 and b-FTTN-PDI4 in diluted chloroform solution (1×10^{-7} M) are shown in **Figure 2b**, and the corresponding optical parameters were summarized in **Table 1**. PDIT shows two main absorption bands centred at 504 and 470 nm corresponding to the 0-0 and 0-1 transitions, respectively. While b-FTTN-PDI4 exhibits absorption peaks ($\lambda_{0-0} = 501$ nm, $\epsilon = 1.28 \times 10^5$ M⁻¹ cm⁻¹; $\lambda_{0-1} = 470$ nm, $\epsilon = 9.8 \times 10^4$ M⁻¹ cm⁻¹) similar to PDIT, a-FTTN-PDI4 shows a slightly hypsochromic shift of its absorption spectrum with enhanced absorption coefficients ($\lambda_{0-0} = 493$ nm, $\epsilon = 1.45 \times 10^5$ M⁻¹ cm⁻¹; $\lambda_{0-1} = 468$

nm, $\epsilon = 1.47 \times 10^5 \text{ M}^{-1} \text{ cm}^{-1}$). In addition, a-FTTN-PDI4 exhibits a broad peak appeared at 550 nm that is absent in the absorption spectra of PDIT and b-FTTN-PDI4. This peak can be assigned as the naphthalene-to-PDIT intramolecular charge transfer (ICT), which can also be found in previous reports on PDI-based molecules with strong ICT features.^{7, 34, 36} Notably, the relative intensity of 0-1 and 0-0 transitions (I_{0-1}/I_{0-0}) is widely regarded as an indicator of the aggregation of PDI chromophores. The I_{0-1}/I_{0-0} ratios of a-FTTN-PDI4, b-FTTN-PDI4 and PDIT amounted to 1.01, 0.76 and 0.64, respectively. The largest I_{0-1}/I_{0-0} ratio of a-FTTN-PDI4 strongly suggests the presence of co-facially π -stacked arrangement and through-space exciton coupling of the PDI chromophores. Furthermore, minimal spectral changes from variant-concentration UV-Vis experiments (concentration = 10^{-4} and 10^{-7} M) were observed for a-FTTN-PDI4, generally indicating no presence of intermolecular aggregation of PDIs (**Figure S4**). This is further supported by their absorption spectra in thin-film state, where the shapes of the spectra changed dramatically from those in the solution states (**Figure S5**). Therefore, we draw the conclusion that the spectral differences between a-FTTN-PDI4 and b-FTTN-PDI4 in solution state originate from the intramolecular π -stacks of the PDI chromophores of a-FTTN-PDI4.

Furthermore, the photoluminescence (PL) properties of the PDI molecules in diluted solution state were studied by steady-state as well as time-resolved techniques. Upon excitation at 500 nm, while PDIT exhibited three distinct vibrionic peaks located at 513, 550 and 593 nm (**Figure 2c**), which is a mirror image of its absorption spectrum and characteristic of emission from isolated molecules. In contrast, both a-FTTN-PDI4 and b-FTTN-PDI4 showed only red-shifted, broad and featureless peaks centred at 607 and 558 nm, respectively. The decay kinetics of these PDI molecules were also probed at 600 nm by time-resolved photoluminescence (TRPL). Similar PL lifetime (τ) of b-FTTN-PDI4 and PDIT were measured to be 1.50 and 1.55 ns, respectively (**Figure 2d**). However, a-FTTN-PDI4 showed a decreased lifetime of 0.99 ns. Such a decreased PL lifetime of a-FTTN-PDI4 was also observed in the thin-film state, which is speculated to originate from the electronic coupling between the co-facially stacked PDI units in a-FTTN-PDI4. (**Figure S5**).

Table 1. Optical and electrochemical properties of a-FTTN-PDI4 and b-FTTN-PDI4.

Acceptor	$\lambda_{\text{abs,sol}}^{\text{a}}$ (nm)	ϵ_{sol} ($\text{M}^{-1}\text{cm}^{-1}$)	$\lambda_{\text{em,sol}}$ (nm)	$E_{\text{g,opt}}^{\text{b}}$ (eV)	LUMO ^c (eV)	HOMO ^d (eV)
----------	---	--	-----------------------------------	---------------------------------------	---------------------------	---------------------------

a-FTTN-PDI4	468,493	1.47×10^5 , 1.45×10^5	608	2.10	-3.64	-5.74
b-FTTN-PDI4	470,501	9.82×10^4 , 1.28×10^5	557	2.23	-3.60	-5.83

^a measured in diluted solution states with a concentration of 10^{-6} M.

^b calculated from the absorption onset of the films.

^c estimated from the reduction onset of the CV curves.

^d estimated from LUMO and $E_{g,opt}$.

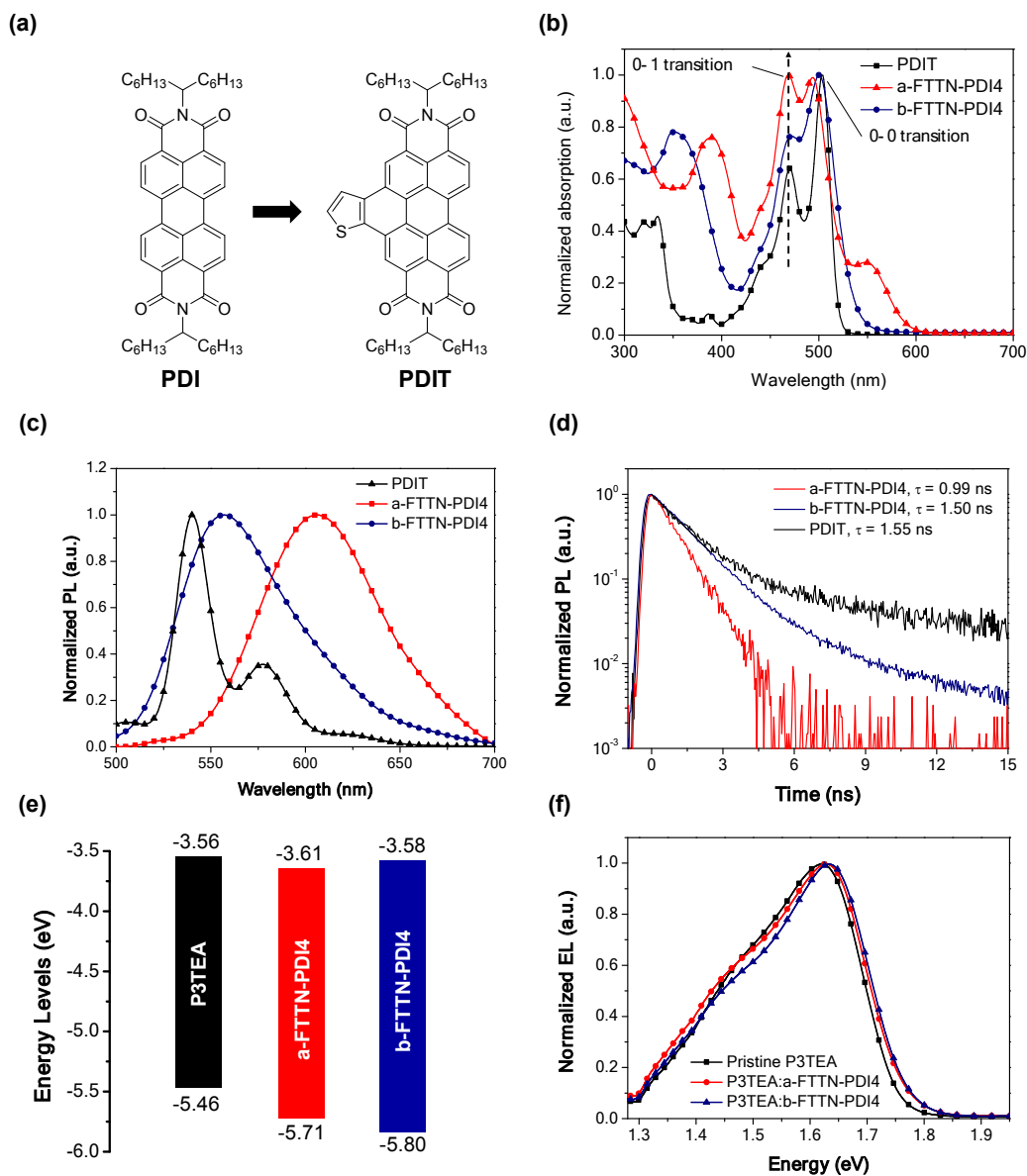


Figure 2. (a) Chemical structure of PDI and PDIT, (b) UV-Vis absorption, and (c) photoluminescence spectra and (d) Time-resolved decay kinetics of a-FTTN-PDI4 and b-FTTN-PDI4 in diluted chloroform solution (10^{-6} M). (e) Energy levels of P3TEA, a-FTTN-PDI4 and b-FTTN-PDI4 measured in solid state. (f) Electroluminescence spectra of the pristine P3TEA, P3TEA:a-FTTN-PDI4 and P3TEA:b-FTTN-PDI4 films.

The electrochemical properties of two SMAs were estimated from cyclic voltammetry measurements in solid state (CV, **Figure S6**) against Fc/Fc⁺ as the external standard, and the results are shown in **Figure 2e**. The LUMO levels of a-FTTN-PDI4 and b-FTTN-PDI4 are estimated from their electron affinities to be -3.61 and -3.58 eV, respectively, which is close to that of the donor polymer P3TEA (-3.56 eV). It is expected that when blending P3TEA and these two SMAs, the energetic offset between the donor and acceptor should be very small. To further prove this, the electroluminescence spectra (EL, **Figure 2f**) of the pristine P3TEA and the blend films were recorded. It was observed that the EL spectra of the blend films showed minimal changes relative to that of the pristine donor polymer, suggesting very small energetic differences between the singlet excited state (S_1) and the charge transfer state (E_{CT}) of the blends, i.e., the charge separation driving forces were negligible. As a result, enhanced V_{OC} and reduced V_{loss} were expected for both blends.

To evaluate the photovoltaic performances of these SMAs, solar cells were fabricated by using the inverted device structure of ITO/ZnO/P3TEA:SMA/MoO₃/Al (**Figure 3a**). The J - V characteristics and the photovoltaic parameters of the optimized devices with the use of thermal annealing and 1,8-octanedithiol as a solvent additive are shown in **Figure 3b** and **Table 2**, respectively. The P3TEA:b-FTTN-PDI4 devices showed the highest PCEs of 7.4% with a V_{OC} of 1.15 V, J_{SC} of 11.5 mA/cm² and FF of 55%, while the P3TEA:a-FTTN-PDI4 devices yielded higher PCEs of 8.6% as a result of simultaneously improved J_{SC} of 12.0 mA/cm² and FF of 61%. It is noted that both devices show good stability under thermal stress, which is one of the advantages of PDI-based materials (**Figure S7**).

The high V_{OC} of the two devices are attributed to the low V_{loss} of 0.57 V (derived from $V_{loss} = E_g/q - V_{OC}$, where E_g is the bandgap of P3TEA of 1.72 eV based on the crossing point between the

absorption and emission spectra), which is the lowest value for efficient PDI-based devices with efficiencies $>7\%$.^{7, 22, 23, 37, 38} On one hand, these low V_{loss} of these two systems are partially attributed to the high-lying E_{CT} that are close to the E_{g} of P3TEA, which minimized the driving force and this part of loss. On the other hand, the non-radiative recombination loss ($\Delta V_{\text{oc,nr}}$) is another important part of voltage losses in the range of 0.34-0.44 V for conventional OSCs, which can be determined by the equation of $q\Delta V_{\text{oc,nr}} = -kT \ln(\text{EQE}_{\text{EL}})$.³⁹ The electroluminescence quantum efficiency (EQE_{EL}) of the a-FTTN-PDI4 and b-FTTN-PDI4 based devices were measured to be 5×10^{-3} , which is one order of magnitude higher than the state-of-the-art SF-PDI₂-based OSCs with a EQE_{EL} of 5×10^{-4} (**Figure 3c**).³⁸ Consequently, a very low non-radiative recombination loss of 0.20 V are estimated for both SMAs, which is one of the lowest $\Delta V_{\text{oc,nr}}$ measured for efficient PDI-based OSCs.^{7, 38, 40, 41} Considering the small driving force and $\Delta V_{\text{oc,nr}}$, it is reasonable that the resulting V_{OC} of the two devices are as high as 1.15 V. Despite the low V_{loss} , the devices still exhibit high EQE of $\sim 60\%$, indicative of efficient charge dissociation and collection of the devices (**Figure 3d**). The enhancement of EQE based on the a-FTTN-PDI4 devices relative to that of the b-FTTN-PDI4 devices are mainly ascribed to the stronger extinction coefficient and improved BHJ morphology, which will be discussed in the later part. The efficient charge dissociation process of the devices was supported by the photoluminescence quenching (PLQ) experiment. High quenching efficiencies of 92% and 94% were measured for the a-FTTN-PDI4 and b-FTTN-PDI4 devices, respectively (**Figure S8**).

Table 2. Photovoltaic parameters of solar cells based on the P3TEA:SMA blends under the illumination of AM1.5G, 100 mW/cm².

	V_{OC}	J_{SC}	FF	PCE ^a	V_{loss}	μ_{h}	μ_{e}	$\mu_{\text{h}}/\mu_{\text{e}}$
	(V)	(mA/cm ²)	(%)	(%)	(eV)	(cm ² /Vs)	(cm ² /Vs)	
a-FTTN-PDI4	1.15±0.01	12.0±0.2	61±1	8.4±0.2 (8.6)	0.57	(2.8±0.2) ×10 ⁻⁴	(2.7±0.3) ×10 ⁻⁴	1.0
b-FTTN-PDI4	1.15±0.01	11.5±0.3	55±1	7.2±0.2 (7.4)	0.57	(3.6±0.1) ×10 ⁻⁴	(2.0±0.2) ×10 ⁻⁴	1.8

^a Average values from 15 devices. The highest PCEs are shown in parentheses.

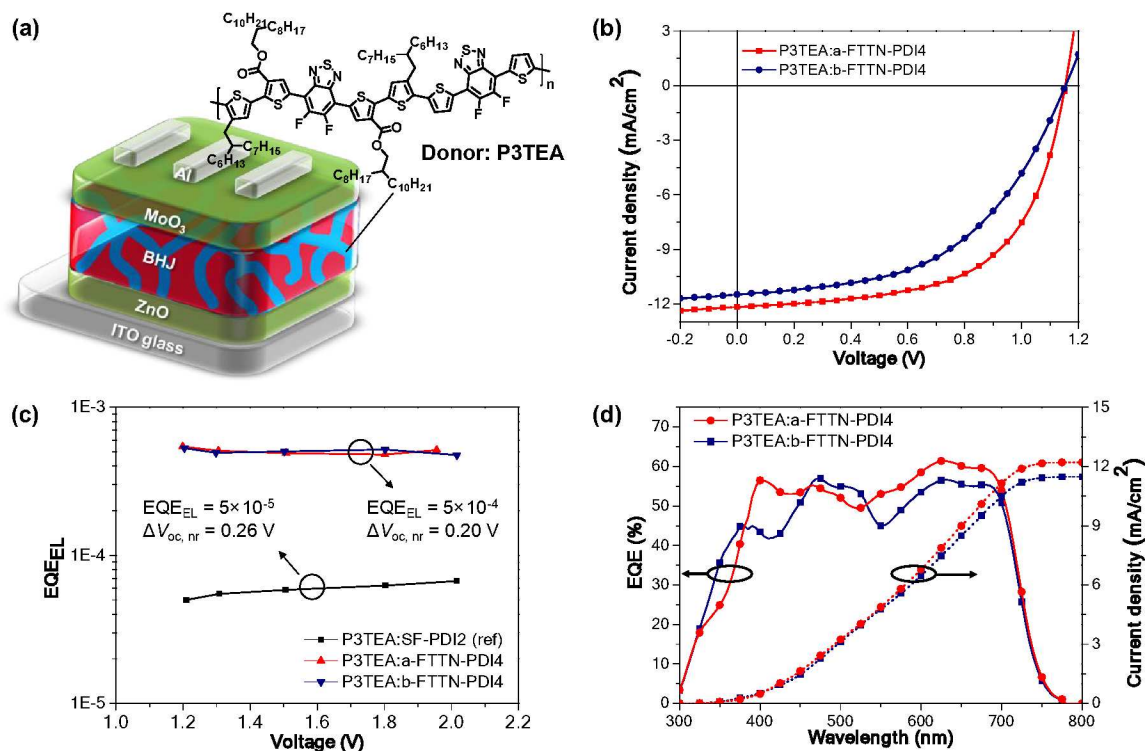


Figure 3. (a) Device architecture and the chemical structure of the P3TEA donor. (b) J - V characteristics of P3TEA:a-FTTN-PDI4 and P3TEA:b-FTTN-PDI4. (c) EQE_{EL} plot of the P3TEA:a-FTTN-PDI4, P3TEA:b-FTTN-PDI4 and the referencing P3TEA:SF-PDI2 system (d) External quantum efficiency curves and the corresponding integrated current density of P3TEA:a-FTTN-PDI4 and P3TEA:b-FTTN-PDI4.

The microstructures of the blend films were probed by grazing incident wide-angle X-ray scattering (GIWAXS). The two-dimensional patterns and the corresponding scattering profiles in the in-plane and out-of-plane direction of the pristine and blend films are depicted in **Figure 4a-e**, and the morphology data are summarized in **Table 3**. Very interestingly, two π - π stacking (010) peaks were fitted for the a-FTTN-PDI4 ($q_z = 1.37$ and 1.70 \AA^{-1} , corresponding to π - π distances of 4.58 and 3.69 \AA , respectively) and b-FTTN-PDI4 ($q_z = 1.33$ and 1.63 \AA^{-1} , corresponding to π - π distances of 4.72 and 3.85 \AA , respectively) pristine films (**Figure S9**). The first π - π stacking peaks with π - π distances larger than 4 \AA are assigned to intermolecular packing of the PDI molecules,

which is consistent with previous reports.^{7, 37, 42} However, it is speculated that the second π - π stacking peaks with π - π distances of 3.6-3.8 Å originate from intramolecular packing, as the π - π distance of the PDI monomer was found to be \sim 3.5 Å depending on different substituents.⁴³ This is consistent with the aforementioned prediction of DFT calculations about the potential intramolecular stacking. Note that the intramolecular stacking peaks are still discernible in the GIWAXS patterns of the blend films. a-FTTN-PDI4 showed a larger coherence length (CL_{010}) of 42.4 Å in the blend film when compared with b-FTTN-PDI4 (15.3 Å), indicating that a-FTTN-PDI4 exhibited a stronger intramolecular π - π stacking tendency than b-FTTN-PDI4. Additionally, the electron mobilities of the a-FTTN-PDI4 obtained from the space-charge-limited current (SCLC) method is indeed higher than that of b-FTTN-PDI4 (2.7×10^{-4} vs. 2.0×10^{-4} cm²/Vs) in the blend films. As a result, the P3TEA:a-FTTN-PDI4 blend achieved a more balance hole/electron mobilities ($\mu_h/\mu_e = 1.0$) compared to the P3TEA:b-FTTN-PDI4 blend ($\mu_h/\mu_e = 1.8$).

In addition, resonant soft X-ray scattering (R-SoXS) was employed to characterize the domain spacing and domain purity of the blend films (**Figure 4f**). Similar domain spacings were determined to be 21.7 and 23.3 nm for the P3TEA:a-FTTN-PDI4 and P3TEA:b-FTTN-PDI4 blend films, under their optimal processing conditions, respectively. The phase segregation is also confirmed by their corresponding atomic force microscopy (AFM) images showing smooth surface morphology with root-mean-square (RMS) roughness of <1 nm (**Figure S10**). Besides, it is widely believed that the domain purity is the key parameter that significantly affects the FF of OSC devices.^{37, 44} The average domain purity derived from integrated scattering intensity of the P3TEA:a-FTTN-PDI4 blend is higher than that of the P3TEA:b-FTTN-PDI4 one (1.00 vs. 0.92). Moreover, suppressed bimolecular recombination was found in the P3TEA:a-FTTN-PDI4 blend, which further supported that the P3TEA:a-FTTN-PDI4 blend exhibit purer domains compared to the P3TEA:b-FTTN-PDI4 one (**Figure S11**). The better molecular packing together with purer domains of the P3TEA:a-FTTN-PDI4 blend account for the higher electron mobilities and thus contribute to the enhanced FFs of the devices, which is in line with the larger extent of intramolecular π -stacking of a-FTTN-PDI4 that facilitates molecular packing and charge transport as discussed above.

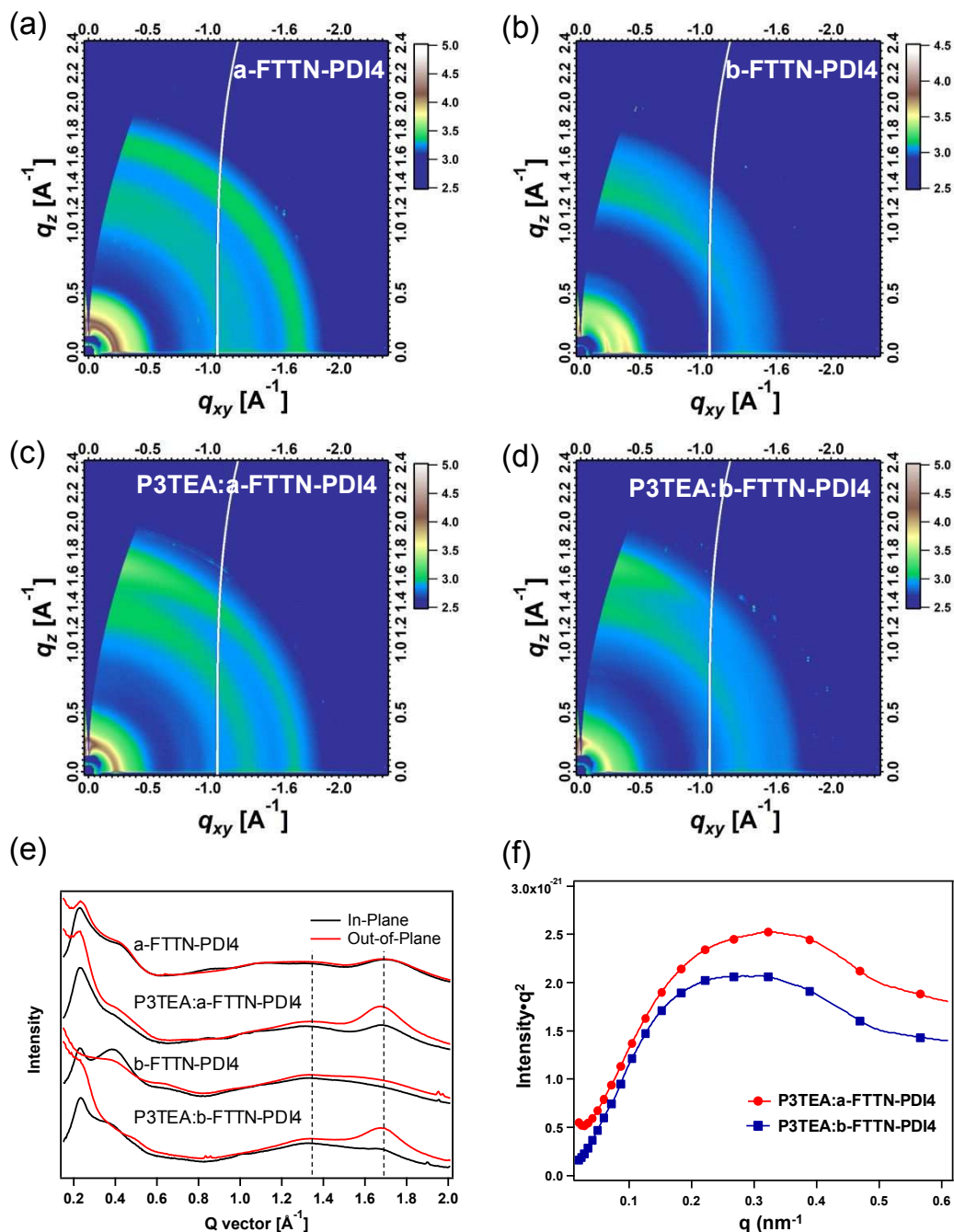


Figure 4. 2D GIWAXS patterns of the (a) a-FTTN-PDI4 and (b) b-FTTN-PDI4 pristine films, (c) P3TEA:a-FTTN-PDI4 and (d) P3TEA:b-FTTN-PDI4 blend films. (e) The corresponding 1D GIWAXS profiles in the in-plane and out-of-plane directions of the blends. (f) Lorentz-corrected and thickness normalized RSoXS profiles of the blends.

Table 3. Summary of morphology data from GIWAXS and RSoXS characterizations based on the pristine SMA films and the P3TEA:SMA blend films.

Material	SMA				Polymer	
	d_{010}	CL_{010}	d_{010}	CL_{010}	d_{010}	CL_{010}
	(Å)	(Å)	(Å)	(Å)	(Å)	(Å)
a-FTTN-PDI4	3.69	19.5	4.58	23.6	/	/
b-FTTN-PDI4	3.85	14.5	4.72	17.7	/	/
P3TEA:a-FTTN-PDI4	3.69	42.4	4.62	15.3	3.76	42.4
P3TEA:b-FTTN-PDI4	3.85	15.3	4.72	23.6	3.76	40.4

Conclusions

In conclusion, we designed and synthesized two isomeric PDI tetramers with different functionalization positions (α - and β -positions) on a naphthalene ring. DFT calculations revealed that a-FTTN-PDI4 featured a “double-decker” geometry in which the adjacent PDI units formed a co-facially stacked alignment, whereas b-FTTN-PDI4 showed relatively less intramolecular stacking. The differences in molecular geometries of a-FTTN-PDI4 from b-FTTN-PDI4 were evidenced by UV-Vis and TRPL. Most importantly, morphology studies revealed that a-FTTN-PDI4 showed better intramolecular and intermolecular packing than those of b-FTTN-PDI4, resulting in higher electron mobilities and FFs. Consequently, the P3TEA:a-FTTN-PDI4 blends exhibited the highest PCE of 8.6%, which outperformed those based on the P3TEA:b-FTTN-PDI4 blends. Efficient charge separation was found despite the high V_{OC} of 1.15 V and a very low non-radiative recombination loss of 0.20 V. The excellent optical and morphological properties of a-FTTN-PDI4 highlight the importance of intramolecular π - π stacking in the design of novel PDI-based SMAs.

Conflicts of interest

The authors declare no competing financial interest.

Acknowledgements

The work described in this paper was partially supported by the National Basic Research Program of China (973 Program project numbers 2013CB834701 and 2014CB643501), the Hong Kong Research Grants Council (project numbers T23-407/13 N, N_HKUST623/13, 16305915, 16322416 and 606012), HK JEBN Limited, HKUST president's office (Project FP201) and the National Science Foundation of China (#21374090). We especially thank Hong Kong Innovation and Technology Commission for the support through projects ITC-CNERC14SC01 and ITS/083/15. D.P acknowledge support from the Croucher Foundation through the Croucher Innovation Grant. X-ray data acquisition and manuscript input by NCSU authors supported by ONR Grant No. N000141512322. X-ray data were acquired at Advanced Light Source, which was supported by the Director, Office of Science, Office of Basic Energy Sciences, of the U.S. Department of Energy under Contract No. DE-AC02-05CH11231.

Reference

1. J. Q. Zhang, H. S. Tan, X. G. Guo, A. Facchetti and H. Yan, *Nat. Energy*, 2018, **3**, 720-731.
2. J. Hou, O. Inganäs, R. H. Friend and F. Gao, *Nat Mater*, 2018, **17**, 119-128.
3. C. Yan, S. Barlow, Z. Wang, H. Yan, A. K. Y. Jen, S. R. Marder and X. Zhan, *Nat. Rev. Mater.*, 2018, **3**, 18003.

4. P. Cheng, G. Li, X. W. Zhan and Y. Yang, *Nat. Photon.*, 2018, **12**, 131-142.
5. A. Wadsworth, M. Moser, A. Marks, M. S. Little, N. Gasparini, C. J. Brabec, D. Baran and I. McCulloch, *Chem Soc Rev*, 2018, DOI: 10.1039/c7cs00892a.
6. G. Zhang, J. Zhao, P. C. Y. Chow, K. Jiang, J. Zhang, Z. Zhu, J. Zhang, F. Huang and H. Yan, *Chem Rev*, 2018, **118**, 3447-3507.
7. J. Zhang, Y. Li, J. Huang, H. Hu, G. Zhang, T. Ma, P. C. Y. Chow, H. Ade, D. Pan and H. Yan, *J. Am. Chem. Soc.*, 2017, **139**, 16092-16095.
8. W. Zhao, S. Li, H. Yao, S. Zhang, Y. Zhang, B. Yang and J. Hou, *J. Am. Chem. Soc.*, 2017, **139**, 7148-7151.
9. Y. Zhong, M. T. Trinh, R. Chen, G. E. Purdum, P. P. Khlyabich, M. Sezen, S. Oh, H. Zhu, B. Fowler, B. Zhang, W. Wang, C. Y. Nam, M. Y. Sfeir, C. T. Black, M. L. Steigerwald, Y. L. Loo, F. Ng, X. Y. Zhu and C. Nuckolls, *Nat Commun*, 2015, **6**, 8242.
10. Y. Z. Lin, Z. G. Zhang, H. T. Bai, J. Y. Wang, Y. H. Yao, Y. F. Li, D. B. Zhu and X. W. Zhan, *Energy Environ. Sci.*, 2015, **8**, 610-616.
11. H. Yao, Y. Cui, R. Yu, B. Gao, H. Zhang and J. Hou, *Angew Chem Int Ed Engl*, 2017, **56**, 3045-3049.
12. L. Meng, Y. Zhang, X. Wan, C. Li, X. Zhang, Y. Wang, X. Ke, Z. Xiao, L. Ding, R. Xia, H. L. Yip, Y. Cao and Y. Chen, *Science*, 2018, **361**, 1094-1098.
13. H. Zhang, H. Yao, J. Hou, J. Zhu, J. Zhang, W. Li, R. Yu, B. Gao, S. Zhang and J. Hou, *Adv. Mater.*, 2018, **30**, 1800613.
14. F. Wurthner, C. R. Saha-Moller, B. Fimmel, S. Ogi, P. Leowanawat and D. Schmidt, *Chem Rev*, 2016, **116**, 962-1052.
15. T. Weil, T. Vosch, J. Hofkens, K. Peneva and K. Mullen, *Angew Chem Int Ed Engl*, 2010, **49**, 9068-9093.
16. X. Guo, A. Facchetti and T. J. Marks, *Chem Rev*, 2014, **114**, 8943-9021.
17. X. Zhan, A. Facchetti, S. Barlow, T. J. Marks, M. A. Ratner, M. R. Wasielewski and S. R. Marder, *Adv. Mater.*, 2011, **23**, 268-284.
18. Y. Lin, Y. Wang, J. Wang, J. Hou, Y. Li, D. Zhu and X. Zhan, *Adv. Mater.*, 2014, **26**, 5137-5142.

19. Y. Liu, C. Mu, K. Jiang, J. Zhao, Y. Li, L. Zhang, Z. Li, J. Y. Lai, H. Hu, T. Ma, R. Hu, D. Yu, X. Huang, B. Z. Tang and H. Yan, *Adv. Mater.*, 2015, **27**, 1015-1020.
20. H. Lin, S. Chen, H. Hu, L. Zhang, T. Ma, J. Y. Lai, Z. Li, A. Qin, X. Huang, B. Tang and H. Yan, *Adv. Mater.*, 2016, **28**, 8546-8551.
21. S. Y. Liu, C. H. Wu, C. Z. Li, S. Q. Liu, K. H. Wei, H. Z. Chen and A. K. Jen, *Adv Sci (Weinh)*, 2015, **2**, 1500014.
22. Q. Wu, D. Zhao, A. M. Schneider, W. Chen and L. Yu, *J. Am. Chem. Soc.*, 2016, **138**, 7248-7251.
23. D. Meng, H. Fu, C. Xiao, X. Meng, T. Winands, W. Ma, W. Wei, B. Fan, L. Huo, N. L. Doltsinis, Y. Li, Y. Sun and Z. Wang, *J. Am. Chem. Soc.*, 2016, **138**, 10184-10190.
24. S. Rajaram, R. Shivanna, S. K. Kandappa and K. S. Narayan, *J Phys Chem Lett*, 2012, **3**, 2405-2408.
25. V. Coropceanu, J. Cornil, D. A. da Silva Filho, Y. Olivier, R. Silbey and J. L. Bredas, *Chem Rev*, 2007, **107**, 926-952.
26. Y. Guo, G. Han, R. Duan, H. Geng and Y. Yi, *J. Mater. Chem. A*, 2018, **6**, 14224-14230.
27. N. J. Hestand and F. C. Spano, *Chem Rev*, 2018, **118**, 7069-7163.
28. J. J. Han, W. Wang and A. D. Q. Li, *J. Am. Chem. Soc.*, 2006, **128**, 672-673.
29. D. Veldman, S. M. Chopin, S. C. Meskers, M. M. Groeneveld, R. M. Williams and R. A. Janssen, *J Phys Chem A*, 2008, **112**, 5846-5857.
30. E. A. Margulies, L. E. Shoer, S. W. Eaton and M. R. Wasielewski, *Phys Chem Chem Phys*, 2014, **16**, 23735-23742.
31. C. Kaufmann, D. Bialas, M. Stolte and F. Wurthner, *J. Am. Chem. Soc.*, 2018, **140**, 9986-9995.
32. K. M. Lefler, K. E. Brown, W. A. Salamant, S. M. Dyar, K. E. Knowles and M. R. Wasielewski, *J Phys Chem A*, 2013, **117**, 10333-10345.
33. E. A. Margulies, C. E. Miller, Y. Wu, L. Ma, G. C. Schatz, R. M. Young and M. R. Wasielewski, *Nat Chem*, 2016, **8**, 1120-1125.
34. N. J. Schuster, D. W. Paley, S. Jockusch, F. Ng, M. L. Steigerwald and C. Nuckolls, *Angew Chem Int Ed Engl*, 2016, **55**, 13519-13523.

35. R. L. Clough and J. D. Roberts, *J Org Chem*, 1978, **43**, 1328-1331.
36. S. X. Li, W. Q. Liu, C. Z. Li, T. K. Lau, X. H. Lu, M. M. Shi and H. Z. Chen, *J. Mater. Chem. A*, 2016, **4**, 14983-14987.
37. H. W. Hu, Y. K. Li, J. Q. Zhang, Z. X. Peng, L. K. Ma, J. M. Xin, J. C. Huang, T. X. Ma, K. Jiang, G. Y. Zhang, W. Ma, H. Ade and H. Yan, *Adv. Energy Mater.*, 2018, **8**, 1800234.
38. J. Liu, S. S. Chen, D. P. Qian, B. Gautam, G. F. Yang, J. B. Zhao, J. Bergqvist, F. L. Zhang, W. Ma, H. Ade, O. Inganäs, K. Gundogdu, F. Gao and H. Yan, *Nat. Energy*, 2016, **1**, 16089.
39. J. Z. Yao, T. Kirchartz, M. S. Vezié, M. A. Faist, W. Gong, Z. C. He, H. B. Wu, J. Troughton, T. Watson, D. Bryant and J. Nelson, *Phys Rev Appl*, 2015, **4**, 014020.
40. X. Liu, X. Du, J. Wang, C. Duan, X. Tang, T. Heumueller, G. Liu, Y. Li, Z. Wang, J. Wang, F. Liu, N. Li, C. J. Brabec, F. Huang and Y. Cao, *Adv. Energy Mater.*, 2018, **8**.
41. H. T. Fu, Y. M. Wang, D. Meng, Z. T. Ma, Y. Li, F. Gao, Z. H. Wang and Y. M. Sun, *ACS Energy Letters*, 2018, **3**, 2729-2735.
42. Q. H. Wu, D. L. Zhao, J. H. Yang, V. Sharapov, Z. Cai, L. W. Li, N. Zhang, A. Neshchadin, W. Chen and L. P. Yu, *Chem. Mater.*, 2017, **29**, 1127-1133.
43. F. Nolde, W. Pisula, S. Müller, C. Kohl and K. Mullen, *Chem. Mater.*, 2006, **18**, 3715-3725.
44. S. Mukherjee, C. M. Proctor, G. C. Bazan, T. Q. Nguyen and H. Ade, *Adv. Energy Mater.*, 2015, **5**, 1500877.